

A Medium Survey of the Hard X-Ray Sky with ASCA. II.: The Source's Broad Band X-Ray Spectral Properties

Roberto Della Ceca¹, GianMarco Castelli¹, Valentina Braito^{1,2}, Ilaria Cagnoni³ and
Tommaso Maccacaro¹

Received : January 15, 1999; accepted : March 29, 1999

Astrophysical Journal, in press

¹Osservatorio Astronomico di Brera, via Brera 28, 20121 Milano, Italy. E-mail:
rdc@brera.mi.astro.it; tommaso@brera.mi.astro.it

²Università degli Studi di Milano, via Celoria 16, 20133 Milano, Italy.

³International School for Advanced Studies, SISSA, via Beirut 2-4, 34014 Trieste, Italy.

ABSTRACT

A complete sample of 60 serendipitous hard X-ray sources with flux in the range $\sim 1 \times 10^{-13}$ ergs cm^{-2} s^{-1} to $\sim 4 \times 10^{-12}$ ergs cm^{-2} s^{-1} (2 - 10 keV), detected in 87 ASCA GIS2 images, was recently presented in literature. Using this sample it was possible to extend the description of the 2-10 keV LogN(>S)-LogS down to a flux limit of $\sim 6 \times 10^{-14}$ ergs cm^{-2} s^{-1} (the faintest detectable flux), resolving about a quarter of the Cosmic X-ray Background.

In this paper we have combined the ASCA GIS2 and GIS3 data of these sources to investigate their X-ray spectral properties using the “hardness” ratios and the “stacked” spectra method. Because of the sample statistical representativeness, the results presented here, that refer to the faintest hard X-ray sources that can be studied with the current instrumentation, are relevant to the understanding of the CXB and of the AGN unification scheme.

The “stacked” spectra show that the average source’s spectrum hardens towards fainter fluxes: it changes from an energy spectral index $<\alpha_E> = 0.87 \pm 0.08$ for the 20 brightest sources (2-10 keV count rate $\geq 3.9 \times 10^{-3}$ cts s^{-1} ; the ”Bright” sample) to $<\alpha_E> = 0.36 \pm 0.14$ for the remaining 40 fainter sources (the ”Faint” sample). The dividing line of 3.9×10^{-3} cts s^{-1} corrispond to unabsorbed 2-10 keV fluxes in the range $\sim 5.4 \times 10^{-13}$ to $\sim 3.1 \times 10^{-13}$ ergs cm^{-2} s^{-1} for a source described by a power law model with energy spectral index between 0.0 and 2.0, respectively. It thus seems that we are now beginning to detect those sources that have the “correct” spectral shape to be responsible for the 2-10 keV CXB.

The hardness ratios analysis indicate that this flattening is due to a population of sources with very hard spectra showing up in the Faint sample; about half of the sources in this sample require $\alpha_E \lesssim 0.5$ while only $\sim 10\%$

of the sources in the brighter sample are consistent with an energy spectral index so flat. A number of sources ($\sim 30\%$) in the Faint sample seem to be characterized by an apparently “inverted” X-ray spectrum (i.e. $\alpha_E \lesssim 0.0$). These objects are probably extremely absorbed sources, as expected from the CXB synthesis models based on the AGN Unification Scheme, if not a new population of very hard serendipitous sources.

The broad band (0.7 - 10 keV) spectral properties of the selected sources, as inferred from the hardness ratios diagram, seem to be more complex than it is expected from a simple absorbed power-law model. We have thus investigated more complex models, in line with the AGNs Unification Scheme, and we find that these latter models seem to be able to explain the overall spectral properties of this sample; this result seems also suggested by the comparison of the hardness ratio diagram of the serendipitous ASCA sources with that obtained using a sample of nearby and well known Seyfert 1 and Seyfert 2 galaxies observed with ASCA.

Subject headings: diffuse radiation - surveys - X-rays: galaxies - X-rays: general - X-rays: Active Galactic Nuclei

1. Introduction

In the last few years many efforts have been made to understand the origin of the cosmic X-ray background (CXB), discovered more than 35 years ago by Giacconi et al. (1962). One of the competing hypotheses - the truly diffuse emission origin (see e.g. Guilbert and Fabian, 1986) - has been rejected by the small deviation of the cosmic microwave background spectrum from a blackbody shape (Mather et al., 1994). Therefore only the alternative interpretation - the discrete sources origin - is left.

Indeed, ROSAT deep surveys, reaching a source density of $\sim 1000 \text{ deg}^{-2}$ at a limiting flux of $10^{-15} \text{ ergs cm}^{-2} \text{ s}^{-1}$ (Hasinger et al., 1998; McHardy et al., 1998), have already resolved the majority (70–80 %) of the soft ($E < 2 \text{ keV}$) CXB into discrete sources. Spectroscopic observations (Shanks et al., 1991; Boyle et al., 1993, 1994; McHardy et al., 1998; Schmidt et al., 1998) of the sources with fluxes greater than $\sim 5 \times 10^{-15} \text{ ergs cm}^{-2} \text{ s}^{-1}$ have shown that the majority (50 – 80 %) of these objects are broad line AGN at $< z > \sim 1.5$. An important minority (10 – 20 %) of ROSAT sources are spectroscopically identified with X-ray luminous Narrow Emission Line Galaxies (Griffiths et al., 1995, 1996; McHardy et al., 1998), whose real physical nature (obscured AGN, starburst) is at the moment debated in the literature (see e.g. Schmidt et al., 1998). Since their average X-ray spectrum is harder than that of the broad line AGNs (Almaini et al., 1996; Romero-Colmenero et al., 1996) and similar to that of the remaining unresolved CXB, these objects could also be substantial contributors to the CXB at higher energies. About 10% of the ROSAT sources are identified with clusters of galaxies (see e.g. Rosati et al., 1998). Thus, it is clear that the ROSAT satellite has been successful in resolving almost all the soft CXB into discrete sources. Furthermore, optical observations of the faint ROSAT sources has lead to the understanding of the physical nature of the objects contributing to it.

On the contrary, at harder energies, closer to where the bulk of the CXB resides, the

origin of the CXB is still matter of debate. Before the ASCA and Beppo-SAX satellites, which carry the first long lived imaging instruments in the 2-10 keV energy band, surveys in this energy range were made using passively collimated X-ray detectors that, because of their limited spatial resolution, allowed the identification of the brightest X-ray sources only, which represent a very small fraction (< 5%) of the CXB (Piccinotti et al., 1982). The so called “spectral paradox” further complicates the situation: none of the single classes of X-ray emitters in the Piccinotti et al., (1982) sample is characterized by an energy spectral distribution similar to that of the CXB. Due to the lack of faint, large and complete samples of X-ray sources selected in this energy range, the contribution of the different classes of sources to the hard CXB was evaluated through population synthesis models and different classes of X-ray sources were proposed as the major contributors by a number of authors (e.g. starburst galaxies, absorbed AGN, reflection dominated AGN, see e.g. Griffiths and Padovani, 1990; Madau, Ghisellini and Fabian, 1994; Comastri et al., 1995; Zdziarski et al., 1993). Recent results from ASCA and Beppo-SAX observations of individual objects and/or medium-deep survey programs (Bassani et al., 1999; Maiolino et al., 1998a; Turner et al., 1998; Boyle et al., 1998a; 1998b; Akiyama et al., 1998) seem to favor the strongly absorbed AGN hypothesis but deeper investigations are still needed to confirm this scenario.

At the *Osservatorio Astronomico di Brera*, a serendipitous search for hard (2-10 keV band) X-ray sources using data from the GIS2 instrument onboard the ASCA satellite is in progress (Cagnoni, Della Ceca and Maccacaro 1998, hereafter Paper I; Della Ceca et al. 1999, in preparation) with the aim of extending to faint fluxes the census of the X-ray sources shining in the hard X-ray sky. The strategy of the survey, the images and sources selection criteria and the definition of the sky coverage are discussed in Cagnoni, Della Ceca and Maccacaro (1998).

In Paper I, a first sample of 60 serendipitous X-ray sources, detected in 87 GIS2 images

at high galactic latitude ($|b| > 20^\circ$) covering ~ 21 square deg. was presented. This sample has allowed the authors to extend the description of the number-counts relationship down to a flux limit of $\sim 6 \times 10^{-14}$ ergs $\text{cm}^{-2} \text{ s}^{-1}$ (the faintest detectable flux), resolving **directly** about 27% of the (2-10 keV) CXB.

Here we study the spectral properties of the 60 ASCA sources listed in Paper I, combining GIS2 and GIS3 data. We have carried out both an analysis of the “stacked” spectra of the sources in order to investigate the variation of the source’s average spectral properties as a function of the flux, and a “hardness-ratio” (HR) analysis of the single sources. This latter method, which is equivalent to the “color-color” analysis largely used at optical wavelengths, is particularly appropriate when dealing with sources detected at a low signal-to-noise ratio (e.g. Maccacaro et al., 1988; Netzer, Turner and George, 1994). We have defined two independent HR and we have compared the position of the sources in the HR diagram with a grid of theoretical spectral models which are found to describe the X-ray properties of known classes of X-ray emitters.

The paper is organized as follows. In section 2 we present the sample and we define the “Faint” and the “Bright” subsamples. In section 3 we present the data, we discuss the data analysis and we define the two HR used. In section 4 we report the results of the stacked spectra and of the HR analysis and we compare them with those expected from simple spectral models and with the CXB spectra. Summary and conclusions are presented in section 5.

2. Definition of the “Faint” and “Bright” Subsamples

The basic data on the 60 X-ray sources used in this paper are reported in Table 2 of Paper I.

To investigate if the spectral properties of the sources depend on their brightness we have defined two subsamples according to the “corrected” 2-10 keV count rate (hereafter CCR) ⁴.

The 20 brightest sources ($\text{CCR} \geq 3.9 \times 10^{-3} \text{ cts s}^{-1}$) define the “Bright” subsample, while the remaining 40 sources define the “Faint” subsample. The dividing line of $3.9 \times 10^{-3} \text{ cts s}^{-1}$ corresponds to an unabsorbed 2 - 10 keV flux of $\sim 5.4 \times 10^{-13}$ or $\sim 3.1 \times 10^{-13} \text{ ergs cm}^{-2} \text{ s}^{-1}$ for a source described by a power law model with energy spectral index of 0.0 and 2.0, respectively absorbed by a Galactic column density of $3 \times 10^{20} \text{ cm}^{-2}$. We note that the numbers reported above are a very weak function of the Galactic absorbing column density along the line of sight (which ranges from 10^{20} cm^{-2} to $9 \times 10^{20} \text{ cm}^{-2}$ for the present sample).

⁴Due to the vignetting of the XRT and the PSF, a source with a given flux will yield an observed count rate depending on the position of the source in the field of view. With “corrected count rate” we mean the count rate that the source would have had if observed at some reference position in the field of view and within a given extraction region. The definition of the source extraction region and of the reference position in the field of view, used to determine the corrected CCR, are discussed in section 3.2. The CCR used here can be obtained dividing the unabsorbed 2-10 keV flux reported in Paper I by the count rate to flux conversion factor of 1cnt/s (2-10) = $11.46 \times 10^{-11} \text{ ergs cm}^{-2} \text{ s}^{-1}$. This value is appropriate for a power law model with energy spectral index of 0.7, filtered by a Galactic absorbing column density of $3 \times 10^{20} \text{ cm}^{-2}$.

We prefer to use the CCR instead of the flux because the CCR is (once the corrections due to the vignetting and the PSF have been applied) an *observed* quantity and it is independent on the spectral properties of the source; on the contrary the flux is model dependent. In first approximation fainter CCR corresponds to fainter sources.

3. Data analysis

All the ASCA images used in Paper I are now in “REV 2” Processing status (see <http://heasarc.gsfc.nasa.gov/docs/asca/ascarev2.html>), thus in this paper we have used this new revision of the data. Furthermore, in order to improve the statistics, we have combined ⁵ data from the GIS2 and GIS3 instruments as explained below.

Data preparation has been done using version 1.3 of the XSELECT software package and version 4.0 of FTOOLS (supplied by the HEASARC at the Goddard Space Flight Center). Good time intervals were selected applying the “Standard REV 2 Screening” criteria (as reported in chapter 5 of the ASCA Data Reduction Guide, rev 2.0), with the only exception of having used a magnetic cutoff rigidity threshold of 6 GeV c⁻¹ (as done in Paper I). HIGH, MEDIUM and LOW bit rate data were combined together. Spectral analysis (see below) has been performed using version 9.0 of the XSPEC software package. We use the detector Redistribution Matrix Files (RMF) gis2v4_0.rmf and gis3v4_0.rmf.

⁵This combination was possible for all the sources but a0447-0627, a0506-3726, a0506-3742 and a0721+7111. For these 4 sources we have used only the GIS2 data.

3.1. “Stacked” spectra

For each source and for the GIS2 and GIS3 data sets, total counts (source + background) were extracted from a circular extraction region of 2 arcmin radius around the source centroid. Background counts were taken from two circular uncontaminated regions of 3.5 arcmin radius, close to the source, or symmetrically located with respect of the center of the image. Source and background data were extracted in the “Pulse Invariant” (PI) energy channels, which have been corrected for spatial and temporal variations of the detector gain. The Ancillary Response File (ARF) relative to each source was created with version 2.72 of the FTOOLS task ASCAARF⁶ at the location of the individual sources in the detectors.

For each source we have then produced a combined GIS spectrum (adding GIS2 and GIS3 data) and the corresponding background and response matrix files, following the recipe given in the ASCA Data Reduction (rev 2.0) Guide (see section 8.9.2 and 8.9.3 and reference therein). Finally, we have produced the combined spectrum of a) the 20 sources belonging to the Bright Sample and b) the 40 sources of the Faint Sample. We note that each object contributes to the stacked counts at most for 6% in the case of the Faint Sample and at most for 25% in the case of the Bright Sample.

In the spectral analysis, being interested in comparing these stacked spectra with that of the hard CXB, we have considered only the counts in the 2.0 - 10.0 keV energy range. The total net counts in the Bright and Faint sample are about 3400 and 2900 respectively.

⁶ The task ASCAARF (which is part of the FTOOLS software package) is able to produce a position-dependent PSF-corrected effective area, $A(E,x,y,d)$, of the (XRT + GIS2 or XRT + GIS3) combination. The inputs of this task are the position x,y (in detector coordinates) and the dimension d of the source’s extraction region.

The stacked spectra were rebinned to give at least 50 total counts per bin.

3.2. Hardness Ratios

For each source and for the GIS2 and GIS3 data set, source plus background counts were extracted in three energy bands: 0.7-2.0 keV (S band), 2.0-4.0 keV (M band) and 4.0-10.0 keV (H band). The S, M and H spectral regions were selected so as to have similar statistics in each band for the majority of the sources. The background counts have been evaluated by using the two background regions considered above; first, we have normalized the background counts to the source extraction region and then we have averaged them. Net counts in S, M and H have been then obtained for each source by subtracting the corresponding S,M and H normalized background counts from the total ones.

To combine the GIS2 and GIS3 data for each source and to compare our results with those expected from simple models, the net counts obtained must be corrected for the position dependent sensitivity of the GIS detectors (see the discussion in section 2.3 of Paper I). In particular we must: a) define a source extraction region and a reference position in the GIS2 or GIS3 field; b) re-normalize the S,M,H net counts from each source to this region (since sources are detected in different locations of the GIS2 or GIS3 field of view); c) perform the simulations for simple models by using the effective area of this region. We will now discuss these points in turn.

As reference region we have used a source extraction region of 2 arcmin radius at the position $x=137$, $y=116$ for the (XRT + GIS2) combination. Using ASCAARF we have produced the effective area values at the position of each source detected in the GIS2 (GIS3) detector. Using these effective area values and through spectral simulations with XSPEC we have derived the correction factors to be applied to each source in the S, M and H band.

For each source we have then applied these correction factors to the net counts of GIS2 and GIS3 separately. Finally, we have combined the GIS2 and GIS3 corrected net counts for each source. In summary, using this procedure we have first re-normalized the GIS2 and GIS3 data for each source to the reference region separately and then combined them. We note that the applied method is very similar to the “flat field” procedure normally used in the analysis of optical imaging and spectroscopic data.

Using the corrected net counts in the S, M and H band we have then computed for each source two “hardness ratios” defined in the following way:

$$HR1 = \frac{M - S}{M + S} \quad HR2 = \frac{H - M}{H + M}$$

The 68% error bars on HR1 and HR2 have been obtained via Monte Carlo simulations using the total counts, the background counts and the correction factors relative to each source.

Similarly, HR1 and HR2 values expected from simple spectral models (see section 4) have been obtained with XSPEC using the effective area of the reference region.

4. Results

4.1. The Hard Energy Range and the CXB

In this section we discuss the hard (2-10 keV) X-ray average spectrum of the present sample and we compare it with that of the CXB; to this end we use the HR2 values and the “stacked” spectra introduced in section 3.

In figure 1, for all sources, we plot the HR2 value versus the GIS2 CCR; the filled squares represent the sources detected with a signal to noise ratio greater than 4.0 while the

open squares represent the sources detected with a signal to noise ratio between 3.5 and 4.0. The HR2 values are then compared with those expected from a non absorbed power-law model with energy spectral index α_E ($f_X \propto E^{-\alpha_E}$) ranging from -1.0 to 2.0 .

Figure 1 clearly shows a broadening of the HR2 distribution going to fainter CCR; furthermore a flattening of the mean spectrum with decreasing fluxes is evident. A similar broadening and flattening of the HR2 distribution is still detected if only the 40 sources (18 Bright and 22 Faint) detected with a signal to noise ratio greater than 4.0 are used, showing that this result is not due to the sources near the detection threshold limit.

It is worth noting the presence of many sources which seem to be characterized by a very flat 2-10 keV spectrum with $\alpha_E \leq 0.5$ and of a number of sources with “inverted” spectra (i.e. $\alpha_E \leq 0.0$). This is particularly evident in the Faint Sample where about half of the sources seem to be described by $\alpha_E \leq 0.5$ and about 30% by “inverted” spectra. These latter objects could represent a new population of very hard serendipitous sources or, alternatively, a population of very absorbed sources as expected from the CXB synthesis models based on the AGN Unification Scheme.

We have checked whether the observed hardening of the mean spectral index can be attributed to a spectral bias in the source’s selection. Since sources with the same flux but different spectrum will deposit a different number of counts in the detector, it is evident that, as one approaches the flux limit of a survey, sources with a *favourable* spectrum will be detected (and thus included in the sample), while sources with an *unfavourable* spectrum will become increasingly under-represented (see Zamorani et al., 1988 for a discussion of this effect). However, in the case of the ASCA/GIS, this selection effect favours the detection of steep sources, thus giving further support to the reality of our findings ⁷.

⁷As an example, in a 50.000 s observation, a source with 2-10 keV flux = 5×10^{-13} ergs

We note that a population of very hard X-ray sources has been recently suggested also by Giommi et al., 1998 in order to explain the spectral properties of the faint BeppoSAX sources and to reconcile the 2-10 keV LogN(>S)–LogS with the 5-10 keV LogN(>S)–LogS obtained from BeppoSAX data.

To further investigate the flattening of the source’s mean spectral index we have used the “stacked” spectra introduced in section 3.1.

In Table 1 we report the results of the power-law fits to the stacked spectra of the Faint and the Bright sample; the unfolded spectra of the two samples are shown in figure 2 (Bright sample: open squares; Faint sample: filled squares).

As can be seen from the χ^2_ν values reported in Table 1 and from the spectra shown in figure 2, a simple power-law spectral model represents a good description of the stacked spectra of the two samples in the 2-10 keV energy range. The N_H values corresponding to the mean line of sight Galactic absorption for the two independent samples have been used in the fits. However, given the energy range of interest (2.0 - 10.0 keV), the spectra are not significantly affected by the Galactic N_H value. Consistent results are obtained if we use either the lowest or highest (0.7×10^{20} cm $^{-2}$ or 9.06×10^{20} cm $^{-2}$ respectively) Galactic N_H value sampled in the present survey.

It is worth noting that the unfolded spectra of the Faint and the Bright sample reported in figure 2 does not show any compelling evidence of emission lines. A strong emission line should be expected if, for example, sources with a strong Iron emission line

cm $^{-2}$ s $^{-1}$ characterized by an absorbed power-law spectrum with $\alpha_E = 2.0$ and $N_H = 3 \times 10^{20}$ will deposit (at the reference position and inside a region of 2 arcmin radius) ~ 300 (2-10) keV counts while a source with the same flux but power-law spectrum with $\alpha_E = 0.0$ and same N_H will deposit ~ 180 counts.

at 6.4 keV, contributing in a substantial way to the CXB, were strongly clustered at some particular redshift. This subject has been already discussed by Gilli et al., 1999, reaching the conclusion that the maximum contribution of the Iron line to the CXB is less than few percent. The unfolded spectra shown in figure 2 confirm their results.

In Figure 3 the results obtained here are compared with those obtained using data from other satellites or from other ASCA medium-deep survey programs. The best-fit energy index of the Bright sample ($\langle \alpha_E \rangle = 0.87 \pm 0.08$) is in good agreement with the mean spectral properties of the objects in the Ginga and HEAO1 A-2 sample and with the mean spectral properties of the broad line AGNs detected by ROSAT (Almaini et al., 1996; Romero-Colmenero et al., 1996). The Faint sample is best described by $\langle \alpha_E \rangle = 0.36 \pm 0.14$; this is consistent with other ASCA results (Ueda et al., 1998) and with the spectra of the CXB in the 2-10 keV energy range (Marshall et al., 1980; Gendreau et al., 1995). For the purpose of figure 3 we have used a count rate to flux conversion factor adequate for a power law spectral model with $\alpha_E = 0.36$ (Faint sample) or $\alpha_E = 0.87$ (Bright sample).

We have evaluated the influence that the sources with the hardest energy distribution have on the combined spectra. If we exclude the 6 sources with $HR2 > 0.2$ (5 from the Faint sample and 1 from the Bright sample) we find that the combined spectra are still significantly different, being described by a power-law model with $\langle \alpha_E \rangle = 0.53 \pm 0.14$ and $\langle \alpha_E \rangle = 1.04 \pm 0.10$ respectively.

Finally, in the case of the Bright sample two sources contribute about 35% of the total counts; if we exclude these two objects the remaining stacked spectrum is described by a power-law model with $\langle \alpha_E \rangle = 1.00 \pm 0.16$, showing that the inclusion or the exclusion of these two objects do not change any of our results. Note that in the case of the Faint sample each object contributes to the stacked counts at most for 6% or less.

These results clearly show that: a) we have detected a flattening of the source's mean spectral properties toward fainter fluxes and b) we are beginning to detect those X-ray sources having a combined X-ray spectra, consistent with that of the 2 - 10 keV CXB.

4.2. The Broad Band Spectral Properties and the AGN Unification Scheme

In this section we do not intend to derive specific spectral properties and/or parameters for each source; the limited statistics and the complexity of AGNs broad band X-ray spectra (see Mushotzky, Done and Pounds, 1993 for a review of the subject) prevent us from doing so. Rather we regard this sample as representative of the hard X-ray sky and we try to investigate if the currently popular CXB synthesis models based on the AGNs Unification Scheme can describe the overall spectral properties of the ASCA sample as inferred from the hardness ratios. According to the AGNs Unification model for the synthesis of the CXB, a population of unabsorbed (Type 1: $N_H \lesssim 10^{22} \text{ cm}^{-2}$) and absorbed (Type 2: $N_H \gtrsim 10^{22} \text{ cm}^{-2}$) AGNs can reproduce the shape and intensity of the CXB from several keV to ~ 100 keV (see Madau, Ghisellini and Fabian, 1994; Comastri et al., 1995; Maiolino et al., 1998b). Because $\sim 90\%$ of the ASCA sources in this sample ⁸ are expected to be AGNs (see Paper I), in the following we will consider this sample as being well approximated by a population of (Type 1 + Type 2) AGNs with flux above $\sim 1 \times 10^{-13} \text{ ergs cm}^{-2} \text{ s}^{-1}$.

In figure 4 we show (open squares) the position of the sources in the “Hardness Ratio” diagram for the Faint (panel a) and Bright (panel b) sample; in figure 4c we have reported

⁸Up to now 12 sources have been spectroscopically identified. The optical breakdown is the following: 1 star, 2 cluster of galaxies, 7 Broad Line AGNs and 2 Narrow Line AGNs. However we stress that this small sample of identified objects is probably not representative of the whole population.

the 12 sources spectroscopically identified so far (see footnote 8). Also reported in figure 4a,b,c (solid lines) are the loci expected from X-ray spectra described by an absorbed power law model. The energy index of the power law ranges from -1.0 up to 2.0 , while the absorbing column densities ranges from 10^{20} cm^{-2} up to 10^{24} cm^{-2} (see figure 4d); the absorption has been assumed to be at zero redshift (i.e. the sources are supposed to be in the local universe).

Figure 4 clearly shows how the “Hardness Ratio” diagram, combined with spectral simulations, can be used to obtain information on the sources’ X-ray spectral properties, as well as the power of using two hardness ratios to investigate the broad band spectral properties of the sources. If only one ratio is known, say HR2 for example, a source with $\text{HR2} \sim 0 - 0.1$ could be described by an absorbed power law with either energy index of 0.0 and $N_H = 10^{20} \text{ cm}^{-2}$ or energy index of ~ 2.0 and $N_H = 10^{23} \text{ cm}^{-2}$. The use of both HR1 and HR2 allows the ambiguity to be solved.

We note that the hardness ratios computed as described in section 3.2 have not been corrected for the different Galactic absorbing column density along the line of sight of each source. For the present sample this ranges from 10^{20} cm^{-2} to $9 \times 10^{20} \text{ cm}^{-2}$; figure 4 clearly shows that this correction is insignificant.

One of the most striking features of figure 4 is the large spread in HR1 and HR2 displayed by the ASCA sources and the departure from the loci of absorbed, single power law spectra. This implies that the broad band (0.7 - 10 keV) spectrum of the sources is more complex than the simple model of an absorbed power law. In particular the ASCA sources located on the left side of the line representing power laws with $N_H \sim 10^{20} \text{ cm}^{-2}$ (see figure 4d) are not explained within the absorbed power-law model. A similar result is obtained even if the absorbing material is assumed to be at higher redshift e.g. $z = 1$ or 2 .

We note that the object in figure 4b (or 4c) characterized by $\text{HR1} \sim 0.0$ and HR2

~ 0.71 (a1800+6638; its X-ray flux is $\sim 6.5 \times 10^{-13}$ ergs cm^{-2} s^{-1}) is spectroscopically identified with the Seyfert 2 galaxy NGC 6552. The X-ray spectrum of this object (Reynolds et al., 1994 and Fukazawa et al., 1994) is consistent with a model composed of a narrow Gaussian line plus an empirical “leaky-absorber” continuum; the latter is composed by an absorbed power-law and a non absorbed power law having a common photon index. Fukazawa et al. (1994) found that the NGC 6552 spectrum requires a photon index of ~ 1.4 , an absorbing column density of $\sim 6 \times 10^{23}$ cm^{-2} , an uncovered fraction of $\sim 2\%$ and a narrow Gaussian line (consistent with the K_{α} iron emission line at 6.4 keV) having an equivalent width of ~ 0.9 keV.

That the simple absorbed power law model is unable to explain the scatter in the hardness ratios is not surprising given the observational evidence that the broad band X-ray spectra of Type 1 and, even more, of Type 2 AGN are complex and affected by several parameters like, for instance, the viewing angle and the torus thickness (see e.g. Turner et al., 1997; Turner et al., 1998; Maiolino et al., 1998a; Bassani et al., 1999). In particular, for Type 2 AGNs we could have, as a function of the absorbing column density, one of the following three cases:

- 1) $10^{22} \lesssim N_H \lesssim 5 \times 10^{23}$ cm^{-2} . The hard X-ray continuum above a few keV is dominated by the directly-viewed component making the source nucleus visible to the observer and the column density measurable; the reflected/scattered component is starting to become relevant in the soft energy range. In this case the observed spectrum is that of an absorbed Type 1 AGNs with some extra flux at low energies;
- 2) $5 \times 10^{23} \lesssim N_H \lesssim 10^{25}$ cm^{-2} . In this case both the directly-viewed component and the reflected/scattered component are observed and the resulting spectrum becomes very complex.
- 3) $N_H \gtrsim 10^{25}$ cm^{-2} . The torus is very thick. The continuum source is blocked from

direct view up to several tens of keV and the observed spectrum is dominated by the scattered/reflected component. In this case the observed continuum is that of a Type 1 AGNs (in the case of scattering by warm material near the nucleus) or that of a Compton reflected spectrum (in the case of cold reflection from the torus).

Given this spectral complexity we have tested the Hardness Ratios plot against the following simplified AGNs spectral model composed of:

- a) an absorbed power-law spectrum. This component represents the continuum source, i.e. for an absorbing column density of about 10^{20} cm $^{-2}$ this represents the “zero” order continua of a Type 1 object;
- b) a non absorbed power-law component, characterized by the same energy spectral index of the absorbed power-law and by a normalization in the range 1-10% of that of the absorbed power-law component. This component represents the scattered fraction (by warm material) of the nuclear emission along the line of sight; theoretical and observational evidence (see Turner et al., 1997 and reference therein) suggest that this scattered fraction is in the range 1-10%;
- c) a narrow emission line at 6.4 keV, having an equivalent width of 230 eV for low values of N_H ($\sim 10^{20}$ cm $^{-2}$). This component represents the mean equivalent width of the Fe K α emission line in Seyfert 1 galaxies as determined by Nandra et al., 1997 using ASCA data.

In summary, the AGN spectral model used is:

$$S(E) = E^{-\alpha_E} e^{-\sigma_E \times N_H} + K E^{-\alpha_E} + Fe_{6.4keV}$$

where E is the photon energy, α_E is the energy spectral index, σ_E is the energy dependent absorbing cross-section, N_H is the absorbing column density along the line of sight to the nucleus, K is the scattered fraction and $Fe_{6.4keV}$ is the Iron narrow emission line at 6.4 keV.

The above simplified AGNs spectral model is equivalent to the model used, by Fukazawa et al., 1994 in the case of NGC 6552 and, by several authors to describe the “first order” X-ray spectra of Seyfert 2 galaxies (see e.g. Turner et al., 1997).

We have tested this model as a function of α_E , the absorbing column density N_H and the scattered fraction K. Figure 5 shows, as an example, the results of the spectral simulations in the case of local sources ($z \sim 0.0$) with $\alpha_E = 1$ and $K = 0.01$ (filled triangles) or $K = 0.1$ (filled circles). The input spectral models for the case $K = 0.01$ and $\text{Log}N_H = 20, 22, 23, 24$ and 24.5 are also shown.

We would like to stress that using this simplified AGNs spectral model we can go, in a continuous way, from a “first order” Type 1 spectra to a “first order” Type 2 spectra only by changing the N_H parameter. In this respect we note that the equivalent width of the Iron narrow emission line at 6.4 keV (which, as we said, is fixed to 230 eV for $N_H \sim 10^{20} \text{ cm}^{-2}$) is ~ 2 keV when $N_H \sim 3 \times 10^{24} \text{ cm}^{-2}$; this latter value is very similar to that measured in many Seyfert 2 galaxies characterized by a similar value of the absorbing column density (Bassani et al., 1999).

As anticipated at the beginning of this section some qualitative conclusions can be drawn from the results reported in Figure 5. First of all it appears that in the context of this simplified AGN spectral model, and for very high N_H values, we are able to explain the hardness ratios of the objects located on the left side of the dashed line representing unabsorbed power laws. Second, the results reported in Figure 5 seem to indicate that many of the latter objects could be characterized by a very high absorbing column density; if this indication is confirmed by deeper investigation with XMM and AXAF, then the number of Compton “thick” systems could be significantly higher than previously estimated. In the meantime we note that this result is consistent with recent findings obtained by Maiolino et al., 1998a, Bassani et al., 1999 and Risaliti, Maiolino and Salvati, 1999 by studying

the fraction of Compton “thick” systems in a sample of Seyfert 2 galaxies observed with BeppoSAX and/or with ASCA.

Finally, to investigate the Hardness Ratio plot *in a model independent way*, we have used a comparison sample of nearby ($z < 1$) Seyfert 1 and Seyfert 2 galaxies pointed at with ASCA. This sample was selected from a data set of about 300 ASCA pointings that were treated in the same manner (see section 2) and that are used to extend the survey presented in Cagnoni, Della Ceca and Maccacaro (1998). Amongst this restricted ASCA data set we have considered those observations pointed on nearby Seyfert 1 and Seyfert 2 galaxies; furthermore, we have considered only the Seyfert 2 galaxies also reported in Table 1 of Bassani et al., 1999 in order to have an uniform data set on their Compton thickness. The comparison sample is composed of 13 Seyfert 1, 15 Compton thin Seyfert 2 and 7 Compton thick Seyfert 2⁹. The targets were analyzed in the same way as the serendipitous sources, combining the GIS2 and GIS3 data (see section 3.2).

The results are shown in figure 6. The Seyfert 1 galaxies are strongly clustered around the locii representing low N_H values; on the contrary the Seyfert 2 galaxies are characterized by a very large spread in their HR1, HR2 values. In particular many of the Seyfert 2 are located on the left side of the line representing power laws with $N_H \sim 10^{20} \text{ cm}^{-2}$; about a half of these sources have been classified as Compton thick system from Bassani et al., 1999. We are tempted to suggest that also the other half are Compton thick objects, whose

⁹The Seyfert 1 are: NGC 1097, MKN 1040, RE 1034+39, MKN 231, MKN 205, 3C 445, I ZW 1, 2E1615+0611, MKN 478, EXO055620-3820.2, MKN 507, NGC 985, TON 180. The Compton thin Seyfert 2 are: NGC 3079, NGC 4258, NGC 3147, NGC 5252, MKN 463e, NGC 1808, NGC 2992, NGC 1365, NGC 6251, MKN 273, IRAS05189-2524, NGC 1672, PKS B1319-164, MKN 348, NGC 7172. The Compton thick Seyfert 2 are: MKN 3, NGC 6240, NGC 1667, NGC 4968, NGC 1386, MKN 477, NGC 5135.

nature is still unrevealed because of the presently poor data quality. XMM and/or AXAF observations are needed to confirm this suggestion. However, whatever their properties (Compton Thin or Thick) are, the comparison of figures 6 and figures 4a,b strongly suggest that at least some of the serendipitous ASCA sources located on the left side of the dashed line connecting the $N_H = 10^{20}$ values could be Type 2 AGNs.

5. Summary and Conclusion

In this paper we have used ASCA GIS2 and GIS3 data for a complete and well defined sample of 60 hard (2-10 keV) selected sources to study the spectral properties of X-ray sources down to a flux limit of $\sim 10^{-13}$ ergs cm^{-2} s^{-1} . To investigate if the spectral properties of the sources depend on their brightness we have defined two subsamples according to the “corrected” 2-10 keV count rate; the Bright sample is defined by the 20 sources with $\text{CCR} \geq 3.9 \times 10^{-3}$ cts s^{-1} , while the Faint sample is defined by the 40 fainter sources. The dividing line of 3.9×10^{-3} cts s^{-1} correspond to unabsorbed 2-10 keV fluxes in the range $\sim 5.4 \times 10^{-13}$ to $\sim 3.1 \times 10^{-13}$ ergs cm^{-2} s^{-1} for a source described by a power law model with energy spectral index between 0.0 and 2.0, respectively.

The main results of this investigation are the following:

- a) the average (2-10 keV) source’s spectrum hardens towards fainter fluxes. The “stacked” spectra of the sources in the Bright sample is well described by a power-law model with an energy spectral index of $\langle \alpha_E \rangle = 0.87 \pm 0.08$, while the “stacked” spectra of the sources in the Faint sample require $\langle \alpha_E \rangle = 0.36 \pm 0.14$; this means that we are beginning to detect those sources having a combined X-ray spectrum consistent with that of the 2-10 keV CXB.
- b) the hardness ratios analysis shows that this flattening is due to the appearance

of sources with very hard spectra in the Faint sample. About a half of the sources in the latter sample require $\alpha_E \lesssim 0.5$ while only 10% of the brighter sources are consistent with an energy spectral index so flat. Furthermore about 30% of the sources in the Faint sample seem to be characterized by “inverted” ($\alpha_E \lesssim 0.0$) 2-10 keV X-ray spectra. These latter objects could represent a new population of very hard serendipitous sources or, alternatively, a population of very absorbed sources as expected from the CXB synthesis models based on the AGN Unification Scheme (see below).

c) a simple absorbed power-law model is unable to explain the broad band (0.7 - 10 keV) spectral properties of the sources, as inferred from the Hardness Ratios diagram. X-ray spectral models based on the AGNs Unification Scheme seem to be able to explain the overall spectral properties of this sample. This seems also suggested by the comparison of our results with those obtained using a sample of nearby and well known Seyfert 1 and Seyfert 2 galaxies observed with ASCA.

Acknowledgments

We are grateful to L.Bassani for stimulating discussions on the comparison sample of Seyfert galaxies, A.Wolter for a carefull reading of the manuscript and the anonymous referee for useful comments. G.C. acknowledge financial support from the “Fondazione CARIPLO”. This work received partial financial support from the Italian Ministry for University and Research (MURST) under grant Cofin98-02-32. This research has made use of the NASA/IPAC extragalactic database (NED), which is operated by the Jet Propulsion Laboratory, Caltech, under contract with the National Aeronautics and Space Administration. We thank all the members of the ASCA team who operate the satellite and maintain the software data analysis and the archive.

Table 1

Sample	Objects	Net counts	α_E	N_{HGal}	χ^2_ν/ν
(2 - 10) keV					$(10^{20} cm^{-2})$
Faint	40	~ 2900	0.36 ± 0.14	2.75	1.09/105
Bright	20	~ 3400	0.87 ± 0.08	3.66	1.06/82

REFERENCES

Almaini, O., Shanks, T., Boyle, B.J., Griffiths, R.E., Roche, N., Stewart, G.C., and Georgantopoulos, I., 1996, MNRAS, 282, 295.

Akiyama, M., Ohta, K., Yamada, T., et al., 1998, Ap.J., 500, 173.

Bassani, L., Dadina, M., Maiolino, R., Salvati, M., Risaliti, G., Della Ceca, R., Matt, G., & Zamorani, G., 1999, Ap.J., in press.

Boyle, B. J., Griffiths, R. E., Shanks, T., Stewart, G. C. & Georgantopoulos, I., 1993, MNRAS, 260, 49.

Boyle, B. J., Shanks, T., Georgantopoulos, I., Stewart, G. C. & Griffiths, R. E., 1994, MNRAS, 271, 639.

Boyle, B.J., Georgantopoulos, I., Blair, A.J., Stewart, G.C., Griffiths, R.E., Shanks, T., Gunn, K.F., & Almaini, O., 1998a, MNRAS, 296, 1.

Boyle, B.J., Almaini, O., Georgantopoulos, I., Blair, A.J., Stewart, G.C., Griffiths, R.E., Shanks, T., & Gunn, K.F., , 1998b, astro-ph/9804084.

Cagnoni, I., Della Ceca, R., & Maccacaro, T., 1998, Ap.J., 493, 54.

Comastri, A., Setti, G., Zamorani, G. & Hasinger, G., 1995, A&A, 296, 1.

Fukazawa, Y., Makishima, K., Ebisawa, K., et al., 1994, PASJ, 46, L141.

Gendreau, K.C., Mushotzky, R., Fabian, A.C., et al., 1995, PASJ, 47, L5.

Giacconi, R., Gursky, H., Paolini, F. & Rossi, B., 1962, Phys. Rev. Lett. 9, 439.

Gilli, R., Comastri, A., Brunetti, G. & Setti, G., 1999, astro-ph/9902256.

Giommi, P., Fiore, F., Ricci, D., Molendi, S., Maccarone, M.C., & Comastri A., 1998,
astroph/9801222.

Griffiths, R. E. & Padovani, P., 1990, Ap.J., 360, 483.

Griffiths, R. E., Georgantopoulos, I., Boyle, B. J., Stewart, G. C., Shanks, T. & Della Ceca,
R., 1995, MNRAS, 275, 77.

Griffiths, R. E., Della Ceca, R., Georgantopoulos, I., Boyle, B. J., Stewart, G. C., Shanks,
T. & Fruscione, A., 1996, MNRAS, 281, 71.

Guilbert, P.W. & Fabian, A.C., 1986, MNRAS, 220, 439.

Hasinger, G., Burg, R., Giacconi, R., Scmidt, M., Truemper, J., & Zamorani, G., 1998,
A&A, 329, 482.

Maccacaro, T., Gioia, I.M., Wolter, A., Zamorani, G. and Stocke, J.T., 1988, ApJ, 326, 680.

Madau, P., Ghisellini, G. & Fabian, A.C., 1994, MNRAS, 270, L17.

Maiolino, R., Salvati, M., Bassani, L., Dadina, M., Della Ceca, R., Matt, G., Risaliti, G., &
G. Zamorani, 1998a, A&A, 338, 781.

Maiolino, R., Bassani, L., Comastri, A., Dadina, M., Della Ceca, R., Gilli, R., Matt, G.,
Risaliti, G., Salvati, M., & G. Zamorani, 1998b, COSPAR, Japan, July 1998.

Marshall, F. et al., 1980, ApJ, 235, 4.

Mather, J.C., et al., 1994 Ap.J., 420, 439.

McHardy, I.M.M., Jones, L.R., Merrifield, M.R., et al., 1998, MNRAS, 295, 641.

Mushotzky, R.E., Done, C., & Pounds, K.A., 1993, Annu.Rev.Astron.Astrophys., 31,717.

Nandra, K., George, I.M., Mushotzky, R.F., Turner, T.J., & Yaqoob, T., 1997, *Ap.J.*, 477, 602.

Netzer, H., Turner, T., & George, I., 1994, *Ap.J.*, 435, 106.

Piccinotti, G., et al., 1982, *Ap.J.*, 253, 485.

Reynolds, C.S., Fabian, A.C., Makishima, K., Fukazawa, Y., & Tamura, T., 1994, *MNRAS*, 268, L55.

Risaliti, G., Maiolino, R., & Salvati, M., 1999, *astro-ph/9902377*.

Romero-Colmenero, E., Branduardi-Raymont, G., Carrera, F.J., et al., 1996, *MNRAS*, 282, 94.

Rosati, P., Della Ceca, R., Norman, C. & Giacconi, R., 1998, *Ap.J.*, 492, L21.

Schmidt, M., Hasinger, G., Gunn, J., et al., 1998, *A&A*, 329, 495.

Shanks, T., Georgantopoulos, I., Stewart, G. C., Pounds, K. A., Boyle, B. J. & Griffiths, R. E., 1991, *Nature*, 353, 315.

Turner, T.J., George, I.M., Nandra, K., & Mushotzky, R.F., 1997, *Ap.J.*, 488, 164.

Turner, T.J., George, I.M., Nandra, K., & Mushotzky, R.F., 1998, *Ap.J.*, 493, 91.

Ueda, Y., Takahashi, T., Inoue, H., et al., 1998, *Nature*, 391, 866.

Zdziarski, A. A., Zycki, P. T., Svensson, R. & Boldt, E., 1993, *Ap.J.*, 405, 125.

Zamorani, G., Gioia, I.M., Maccacaro, T., & Wolter, A., 1988, *A&A*, 196, 39.

6. Figure Captions:

Figure 1: HR2 value versus the "corrected" 2 - 10 keV count rate for all the serendipitous ASCA sources belonging to the Cagnoni, Della Ceca and Maccacaro, 1998 sample. The filled squares represent the sources detected with a signal to noise ratio greater than 4.0 while the open squares represent the sources detected with a signal to noise ratio between 3.5 and 4.0. The dotted lines represent the expected HR2 values for a non absorbed power-law model with an energy spectral index as indicated in the figure. The dashed line represent the dividing line between the Faint and the Bright sample.

Figure 2: The unfolded stacked ASCA spectrum of the Faint (filled squares) and the Bright (open squares) sample. Note that this spectra are shown in arbitrary units.

Figure 3: Comparison of the results obtained from the stacked spectra of the Faint and the Bright sample with those obtained using data from other satellites or from other ASCA medium-deep survey programs (adapted from figure 3 of Ueda et al., 1998).

Figure 4: a) "Hardness Ratio" distribution for the sources in the Faint sample. The grid represents the locii expected from absorbed power law spectra (values are shown in panel d); b) As panel a but for the Bright sample; c) As panel a but for the identified sources. Symbols are as follows: star: star; filled triangles: clusters of galaxies; filled squares: Narrow Line AGNs; open squares: Broad Line AGNs; d) Expected HR1 and HR2 values as a function of the absorbing column density and of the power law energy index of the spectrum. The absorption is assumed to be at zero redshift.

Figure 5: The open squares represent the position of the sources in the "Hardness Ratio" diagram (Faint + Bright Sample). The solid lines are the locii expected from the simplified AGN spectral model discussed in the text (see section 4.2). We have highlighted with filled dots or filled triangles the absorbing column densities of $\log N_H = 20, 21.5$,

22, 22.5, 23, 23.5, 24, 24.5 (from left to right); the absorption has been assumed to be at zero redshift (i.e. the sources are supposed to be in the local universe). The filled triangles represent the model relative to an energy spectral index equal to 1.0 and scattered fraction of 1%, while the filled dots represent the model relative to an energy spectral index equal to 1.0 and scattered fraction of 10%. The dashed line represents the locus expected from unabsorbed power laws ($N_H \sim 10^{20} \text{ cm}^{-2}$) and energy spectral index ranging from -1.0 up to 2.0 . We also show the input spectral models for the case of $K=10\%$ and $\text{Log}N_H = 20$, 22, 23, 24, and 24.5.

Figure 6: As figure 4a but for the comparison sample of Seyfert 1 and Seyfert 2 galaxies. Filled triangles: Seyfert 1; Open squares: Compton Thick Seyfert 2; Filled Squares: Compton Thin Seyfert 2 (see section 4.2).

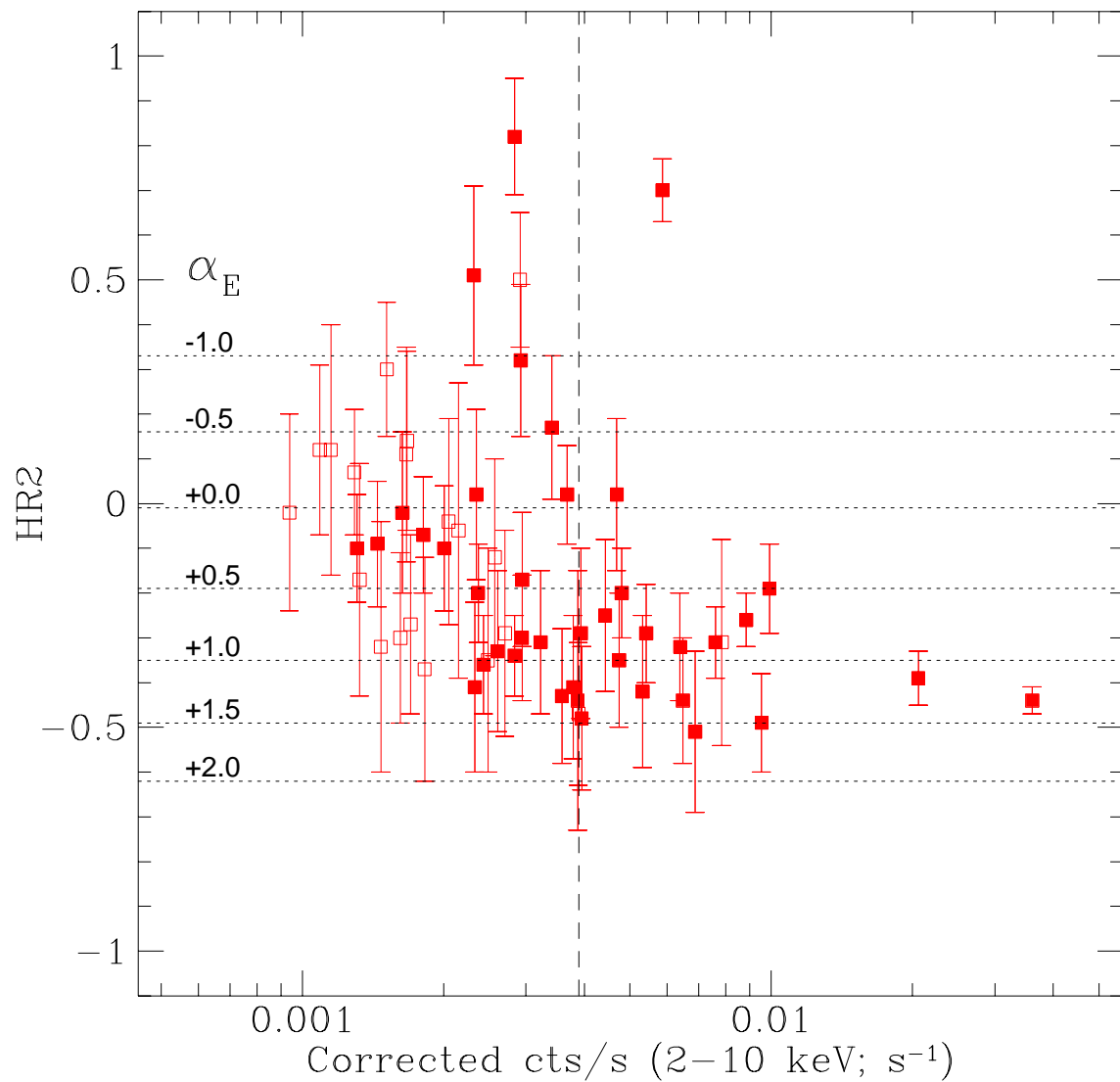


Fig. 1.—

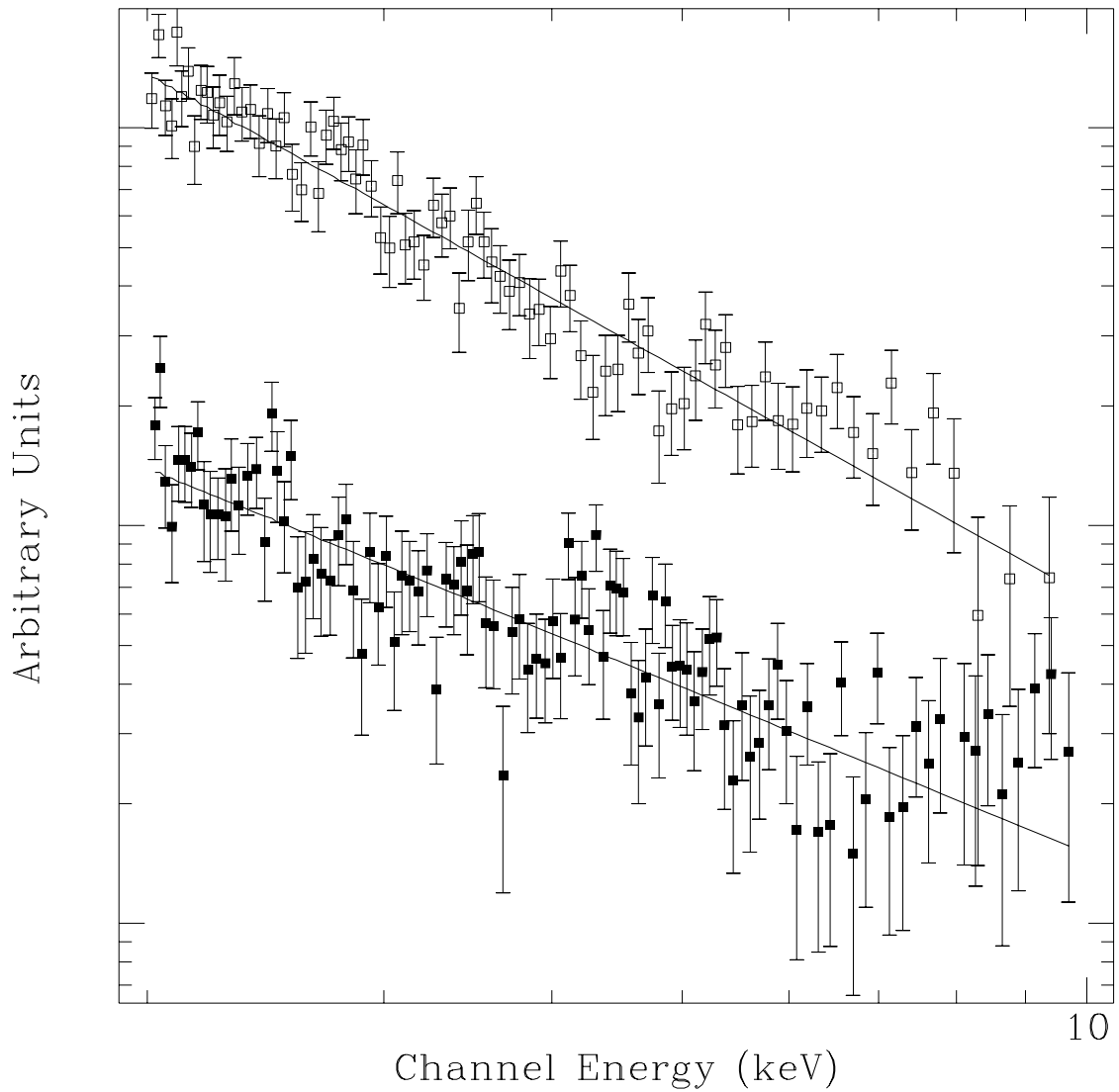


Fig. 2.—

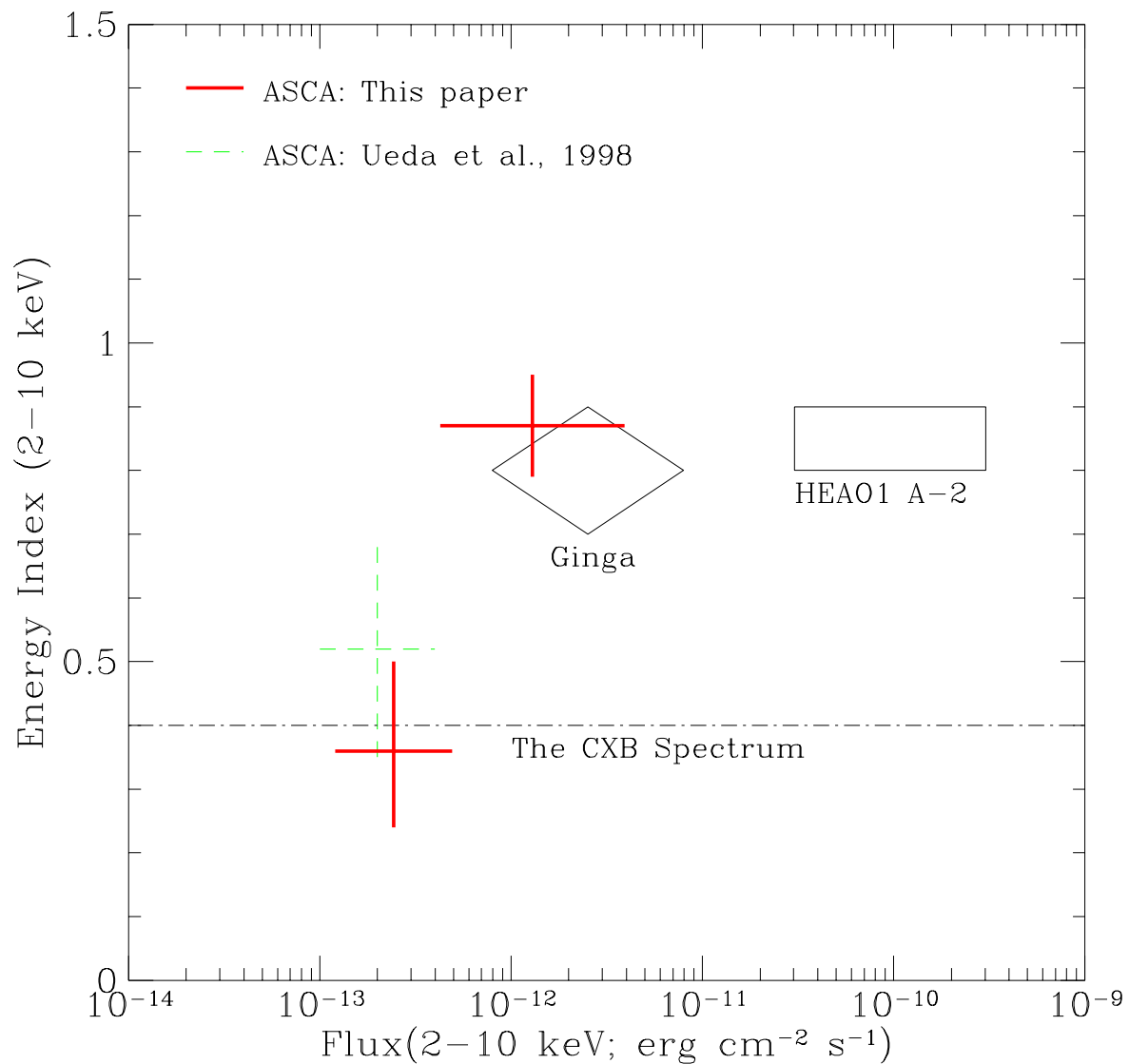
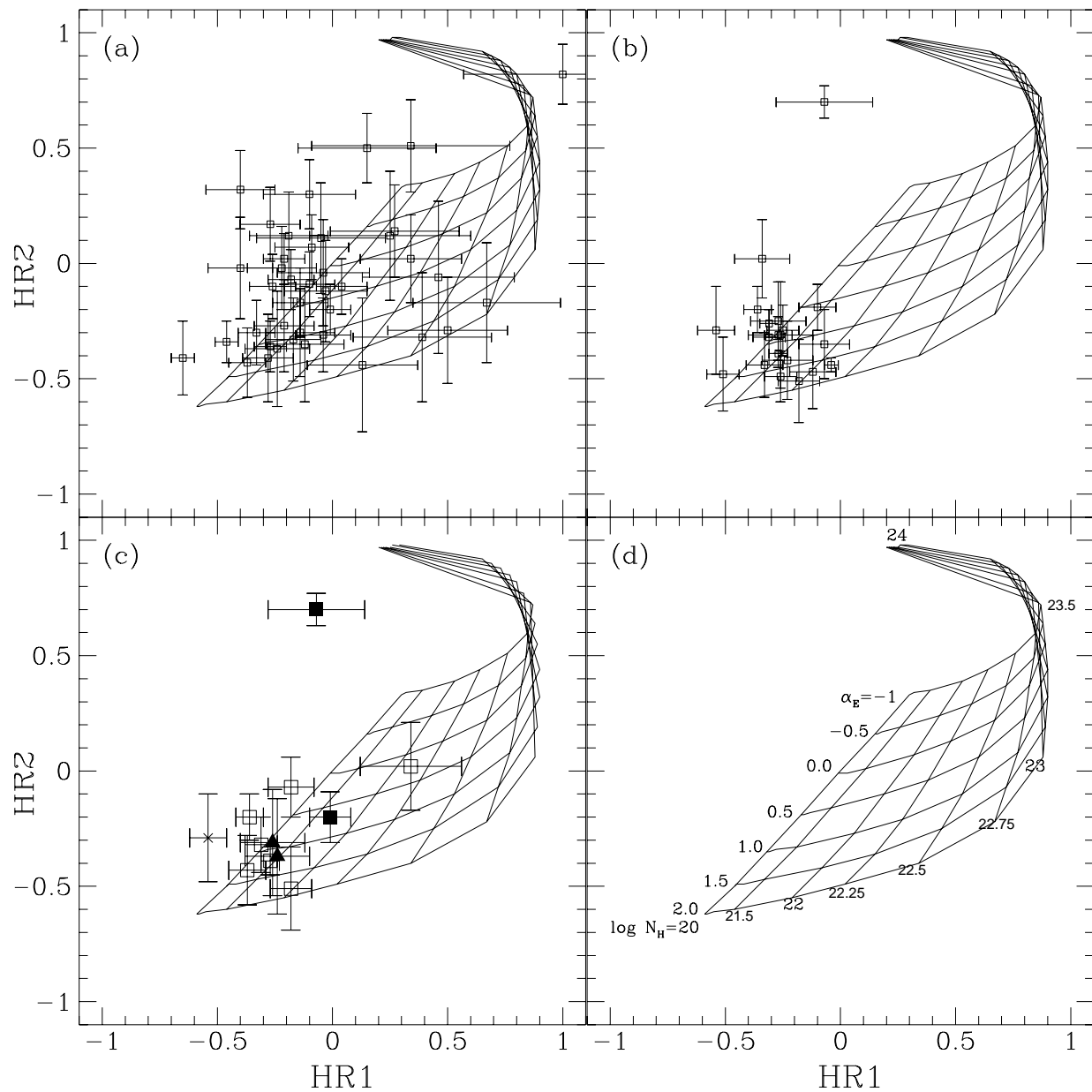


Fig. 3.—



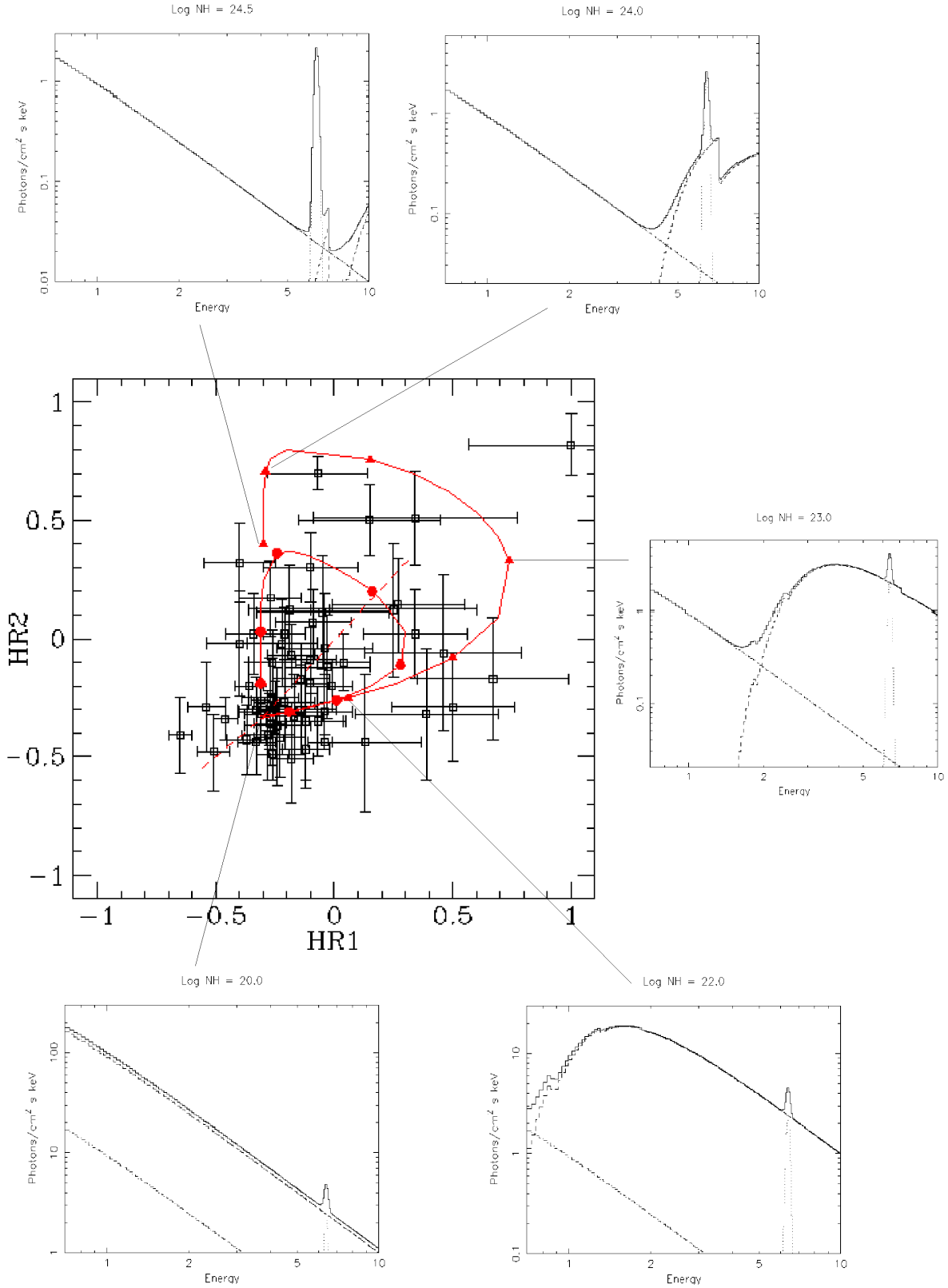


Fig. 5.—

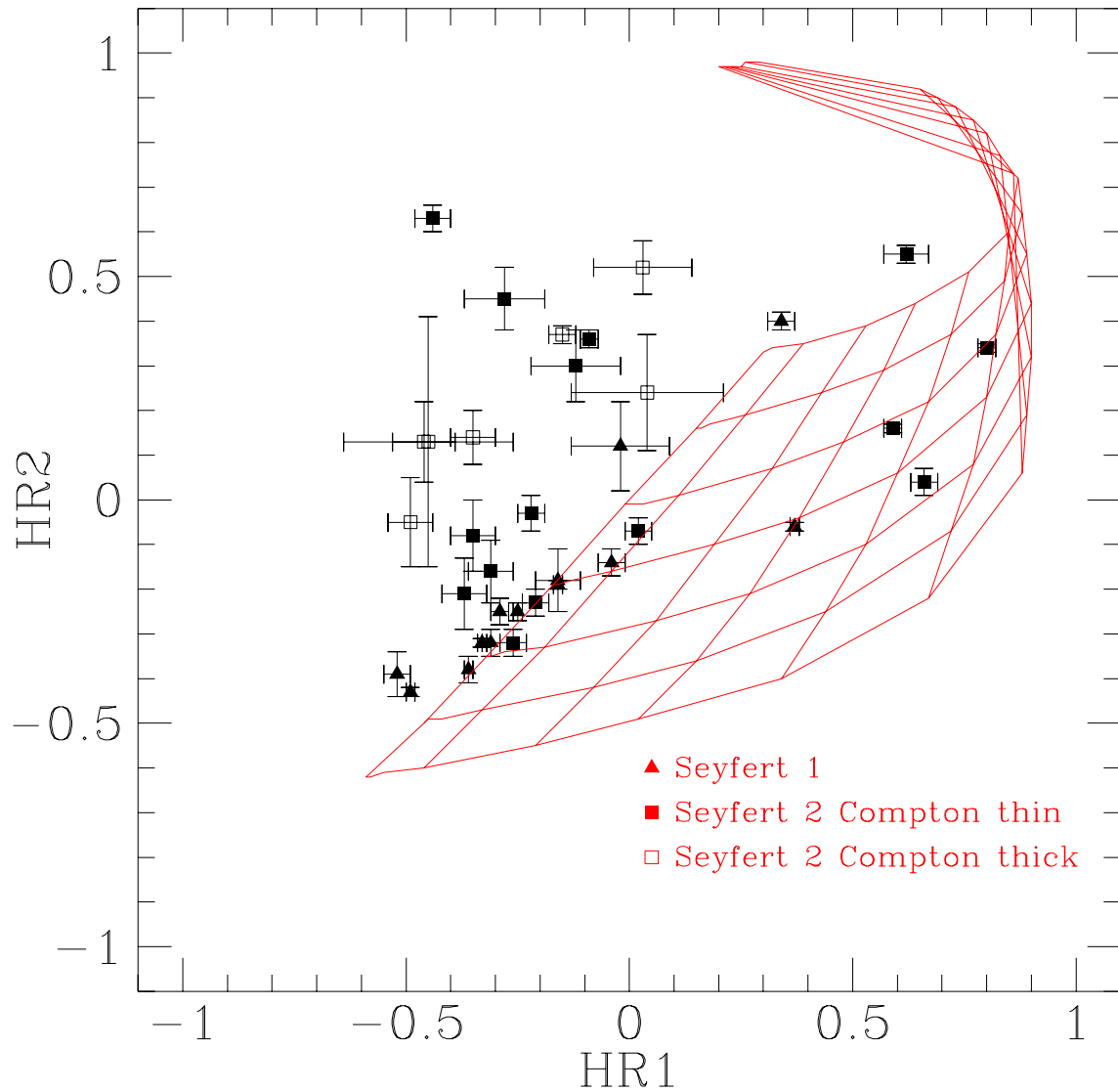


Fig. 6.—